Single-Molecule Biosensors

DOI: 10.1002/anie.201309438

# Point Decoration of Silicon Nanowires: An Approach Toward Single-Molecule Electrical Detection**

*Jindong Wang, Fangxia Shen, Zhenxing Wang, Gen He, Jinwen Qin, Nongyi Cheng, Maosheng Yao,* Lidong Li,* and Xuefeng Guo**

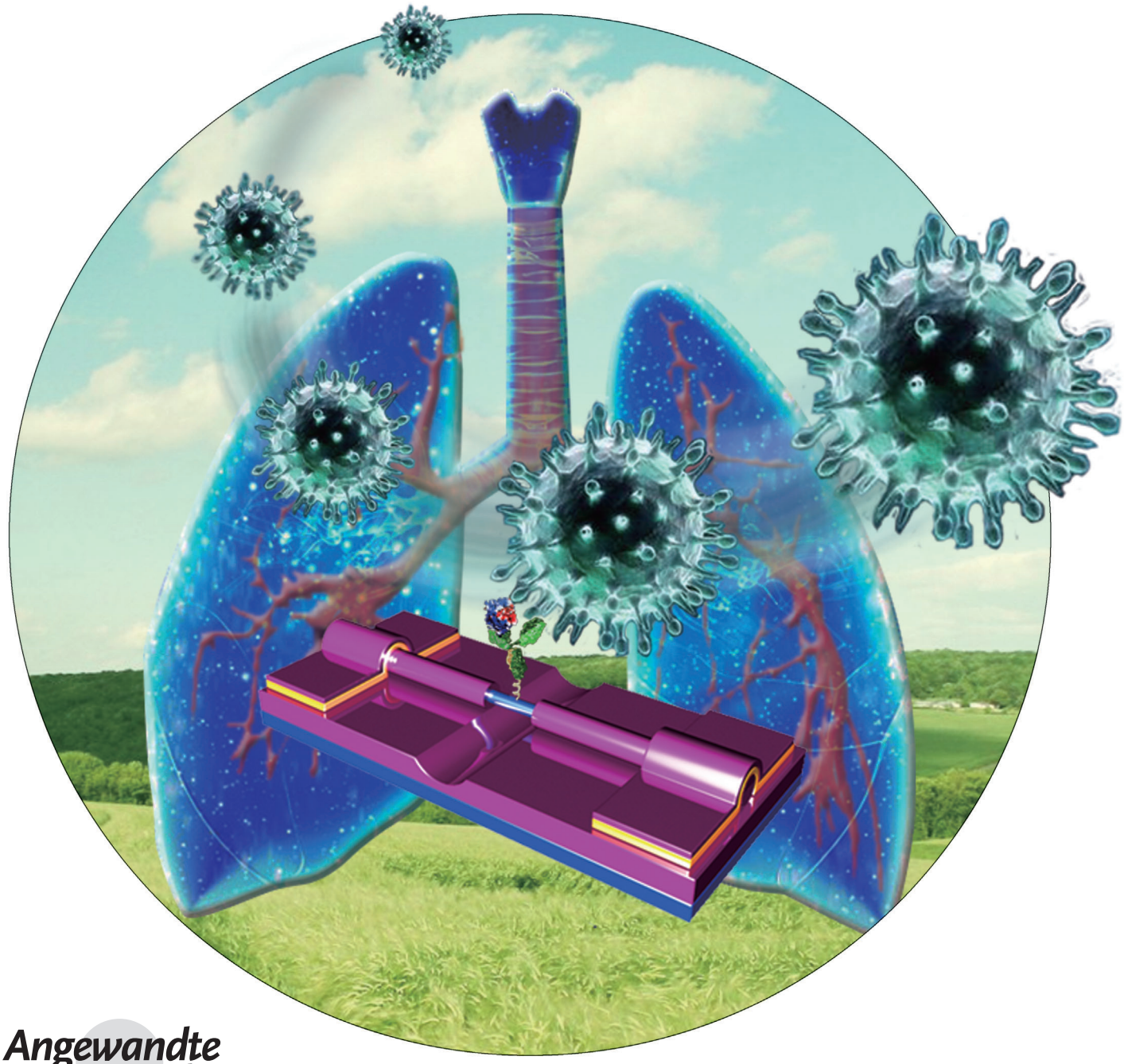

Angewandte International Edition Chemie

***Abstract:*** *Probing interactions of biological systems at the molecular level is of great importance to fundamental biology, diagnosis, and drug discovery. A rational bioassay design of lithographically integrating individual point scattering sites into electrical circuits is capable of realizing real-time, label-free biodetection of influenza H1N1 viruses with single-molecule sensitivity and high selectivity by using silicon nanowires as local reporters in combination with microfluidics. This nanocircuit-based architecture is complementary to more conventional optical techniques, but has the advantages of no bleaching problems and no fluorescent labeling. These advantages offer a promising platform for exploring dynamics of stochastic processes in biological systems and gaining information from genomics to proteomics to improve accurate molecular and even point-of-care clinical diagnosis.*

Establishing a practical platform for electrically probing biomolecular interactions with high selectivity and high sensitivity,[1] with the ultimate goal of detecting single-molecule events,[2] is of great importance to fundamental biology, diagnosis and drug discovery.[3] To this end, several approaches based on nanomaterials and nanostructures have been successfully developed for single-molecule electrical biosensor fabrication, including molecular junctions,[4] silicon nanowires,[5] carbon nanotubes,[6] nanopores/nanoclusters,[7] and others.[8] In this study, we describe another rational bioassay design of lithographically integrating individual point scattering sites into electrical circuits that are capable of realizing real-time, label-free biodetection of influenza H1N1 viruses with single-molecule sensitivity, using silicon nanowires (SiNWs) as local reporters in combination with microfluidics (Figure 1). A feature of particular interest detailed herein is the nature of the one-dimensional (1D) $Si/SiO_2$ core–shell structure of chemical vapor deposition (CVD)-grown SiNWs,[9] which allows us to open functional nanogaps for subsequent biocompatible assembly. In conjunction with other advantages of SiNWs, such as easy availability through bottom-up approaches, superior electrical properties with precise controllability, favorable biocompatibility, size comparability, and flexible surface tailorability, this intrinsic core–shell structure forms the basis for new types of SiNW-based biosensors.[1a,5,10] Along with these, owing to the fact that silicon is the leading material used in today's semiconductor industry, it is natural that 1D SiNWs have become a focus of sensing research, as SiNW-based biosensors have the capability of the integration with the existing silicon industry and processing technology.[1a,5,10,11] On the other hand, influenza (such as H1N1) epidemics worldwide are responsible for million cases of severe illness each year, eventually resulting in substantial economic and human costs annually. However, rapid and reliable virus detection methods are obviously lacking in conventional blood test and symptom observation. Previously, we demonstarted that the use of SiNWs can achieve a detection limit of 29 influenza viruses/μL in diluted clinical exhaled breath,[10b] and $10^4$ viruses/L in air.[10c] However, in certain cases, for example, detecting deadly pathogenic bacterium and binding kinetics, there is a need to monitor the biological event for a single molecule. Therefore, we demonstrate herein that the combination of programmed self-assembly with sophisticated micro/nanofabrication affords unique SiNW-based electrical biosensors that offer direct, rapid single virus detection with high selectivity.

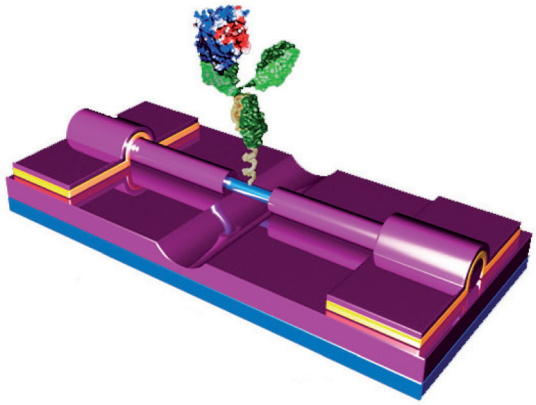

***Figure 1.*** A depiction of single-molecule electrical biosensors formed by point decoration of SiNWs, where metal electrodes are passivated by a thermally deposited 50 nm-thick $SiO_2$ layer.

SiNW-based single-molecule electrical biosensors were fabricated by using a simple three-step process as follows (Figure 2a): SiNW transistor fabrication, gap opening, and point biodecoration. Details can be found in the Supporting Information. This process uses uniform p-type SiNWs of high quality (Supporting Information, Figure S1a) synthesized by an Au-catalyzed vapor–liquid–solid (VLS) method (see the Supporting Information).[12] Transmission electron microscopy (TEM) characterizations reveal that SiNWs have the desired core–shell structure with the single-crystalline core ([011] growth direction) sheathed with on average a 10 nm-thick layer of amorphous $SiO_2$ (Supporting Information, Figure S1b), consistent with previous reports.[9] This unique

[*] J. Wang,[+] Prof. L. Li
School of Materials Science and Engineering
University of Science and Technology Beijing
Beijing 100083 (P. R. China)
E-mail: lidong@mater.ustb.edu.cn

Z. Wang, G. He, J. Qin, N. Cheng, Prof. X. Guo
Center for Nanochemistry, Beijing National Laboratory for Molecular Sciences, State Key Laboratory for Structural Chemistry of Unstable and Stable Species, College of Chemistry and Molecular Engineering, Peking University
Beijing 100871 (P.R. China)
E-mail: guoxf@pku.edu.cn

F. Shen,[+] Prof. M. Yao
State Key Joint Laboratory of Environmental Simulation and Pollution Control, College of Environmental Science and Engineering, Peking University
Beijing 100871 (P.R. China)
E-mail: yao@pku.edu.cn

[+] These authors contributed equally to this work.

[**] We acknowledge primary financial support from NSFC (21225311, 51121091, 21373014, 91333102, 21003002, 21277007, and 41121004) and MOST (2012CB921404).

Supporting information for this article is available on the WWW under http://dx.doi.org/10.1002/anie.201309438.

  

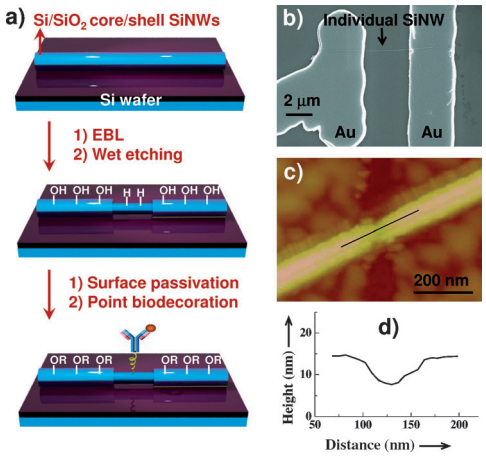


***Figure 2.*** a) A three-step process used for fabricating SiNW-based single-molecule electrical biosensors. b) SEM image of an individual SiNW-based transistor. c), d) AFM image of a typical nanogap and corresponding height profile cross the nanogap.

structure sets the foundation for the following single-molecule biosensing platform development. By using these high-quality crystalline SiNWs, high-density transistor arrays were then made on doped silicon wafers with circa 1000 nm of thermally grown $SiO_2$ on the surface through the combination of microfluidics and photolithography that has been well-developed (Supporting Information, Figure S2a).[10] Figure 2b shows an individual SiNW that nicely spans between metal electrodes with a circa 3 μm space. Electrical characterizations demonstrated that SiNWs show the typical p-type behaviors with good ohmic contacts (Supporting Information, Figure S2b). To rule out potential artifacts from Schottky barrier modification between analytes and metal electrodes, we passivated Au leads by a 50 nm-thick layer of silicon oxide through electron beam thermal evaporation after electrode deposition and before the second lithographic step for gap opening. The diameter of SiNWs used in this study varies in the range of 20–30 nm.

In the second step, we applied high-resolution electron beam lithography (EBL) by a DesignCAD file (5 nm wide and 150 μm long, well-separated from electrodes) to open a narrow window perpendicular to SiNWs on the surface of a spin-cast layer of polymethylmethacrylate (PMMA).[4a,d,e,13] Then we carried out subsequent chemical wet etching by a HF/$NH_4F$ buffer solution through the window to expose the crystalline silicon core of SiNWs by removing the amorphous $SiO_2$ sheath (Figure 2a, middle). The outcome of this etching progress is the formation of the hydrogen-terminated silicon trench in the nanoscale size that is comparable to that of antibody, which is of crucial importance to single-molecule detection. To ensure the success, we investigated the time dependence of the etching process by using the relatively gentle etching mixture solution (40% HF/40% $NH_4F$ = 1:7). We immersed different silicon wafers with 1000 nm of thermally grown $SiO_2$ on the surface, which have a 1 μm-wide window opened, into the HF buffer solution for 10 s, 60 s, and 90 s, respectively. This treatment afforded the corresponding etching depths of circa 11 nm for 10 s, circa 55 nm for 60 s, and circa 88 nm for 90 s, as demonstrated by atomic force microscopic (AFM) measurements (Supporting Information, Figure S3). We found that the relationship between the etching depth and the etching time fits a linear model (Supporting Information, Figure S4): $y = vx$,[14] where y is the etching depth, $x$ the etching time, and $v$ the etching rate. Therefore, the calculated etching rate in our case approaches about 1 nm $s^{-1}$. Considering the thickness of the $SiO_2$ layer of SiNWs used, we then fixed the etching time at about 10 s for all the following experiments. Figure 2c shows a typical AFM image obtained under optimized etching conditions. We take the image convolution of the AFM tip size into consideration and set the upper bound on the size of a typical gap opened in the SiNWs of about 45 nm. According to the thickness of the $SiO_2$ shell (ca. 8 nm; Figure 2d), therefore, we estimated the actual nanogap, where the surface of the crystalline silicon core is completely open, to be about 30 nm. This value is only large enough for accommodation of a single (or at most two) H1N1 antibodies (ca. 20 nm).[15] Another remarkable feature from this step is to produce two distinct surfaces with different reaction activities: hydrogen-terminated silicon surface and hydroxy-terminated $SiO_2$ surface (Figure 2a, middle), thus rendering the ability of direct chemical assembly as demonstrated in the third step.

The purpose of the third step is to incorporate a single H1N1 antibody into the nanogap through programmed point decoration (Figure 2a, bottom). The major reaction we utilized here is photochemical hydrosilylation (Figure 3a), which is a classical radical-based addition.[16] To preclude the quenching effect of reactive hydroxy groups from the $SiO_2$ surface on the radicals, we used octadecyltrichlorosilane (OTS), a typical reagent used for reducing the $SiO_2$ dielectric traps and tuning the surface energy,[17] to form a passivated self-assembled monolayer (SAM). As a result, photochemical hydrosilylation is selectively confined at the nanogapped area. Furthermore, we chose photochemical hydrosilylation as the surface reaction because of its cleanness in comparison with other Si–H functionalization methods.[18] These methods require either Lewis acid catalysts or free-radical initiators, which potentially influence both the stability of proteins and the intrinsic electrical properties of SiNWs. To prove the efficiency, we first used naked silicon wafers without $SiO_2$ on the surface to follow the reactions (Figure 3a) (details can be found in the Supporting Information). Bare silicon wafers were obtained by immersing them into the HF solution for 20 min for entirely removing $SiO_2$. This forms the hydrogen-terminated surface with the characteristic Si–H stretch at about 2108 $cm^{-1}$, as evidenced by FTIR spectroscopy (Supporting Information, Figure S5a).[16c] However, after the surface reaction between Si–H and propargylamine (Figure 3a), we observed the intensity decrease of the Si–H stretch but the appearance of the new stretching modes at about 1648 $cm^{-1}$, 1450 $cm^{-1}$, 2960 $cm^{-1}$, and 3220 $cm^{-1}$ (Figure 3b; Supporting Information, Figure S5b). These modes should be assigned to C=C, $CH_2$ (bending), $CH_2$ (stretching), and amine groups,[18a,19] respectively, thus proving the occurrence of alkyne hydrosilylation. Further X-ray photoelectron spectroscopy (XPS) measurements strengthened this fact. In comparison with the XPS spectra on bare hydrogen-termi-

  

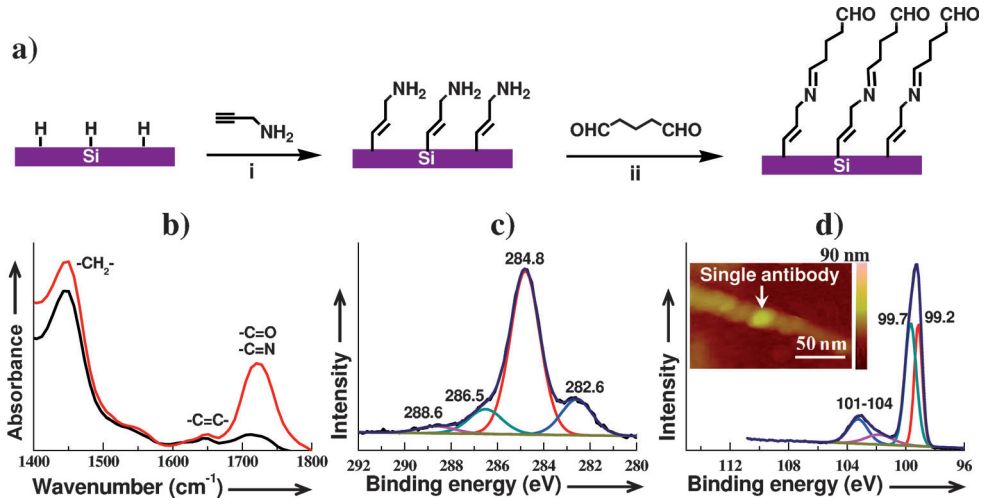


***Figure 3.*** a) Demonstration of the strategy used for surface functionalization. b) FTIR spectra of bare silicon wafers after alkyne hydrosilylation (black) and further condensation (red). c), d) High-resolution C 1s and Si 2p XPS spectra after alkyne hydrosilylation. Inset in (d) shows an AFM image after H1N1 antibody attachment.

nated silicon surfaces (Supporting Information, Figure S5c,d), there is a clear indication of the emergence of the C 1s and Si 2p peaks after propargylamine grafting. As shown in Figure 3c,d, the newly-formed C 1s and Si 2p peaks with the binding energies of 282.6 eV and 99.7 eV are characteristic of carbon and silicon, respectively, in Si–C bonds that definitely result from the surface reaction of alkyne hydrosilylation. Therefore, the execution of alkyne hydrosilylation successfully produces the Si–C linkage on the substrate surface, thus leaving the surface-bound amino groups available for subsequent reactions. The other three peaks in Figure 3c, namely 284.8 eV (C=C), 286.5 eV (C=O and/or C–N) and 288.6 eV (C(O)O), may originate from carbon atoms from reacted propargylamine and/or external contamination (Supporting Information, Figure S5b). In Figure 3d, the peak with a binding energy of 99.2 eV should be assigned to Si–Si bonds in silicon wafers and the 101–104 eV region should be related to oxide or suboxide species on the silicon surface (Supporting Information, Figure S5d). These results are similar to the previous observations.[1g,16c,20] After rinsing by copious dichloromethane, the amino-terminated surface was then soaked into the glutaraldehyde solution. The IR spectrum shows the loss of the amine stretch at about 3220 $cm^{-1}$ and the appearance of the new C=N (and/or C=O) stretches at about 1720 $cm^{-1}$ (Figure 3b).[19b,21] These observations should be due to the imine linkage formation through condensation between surface-bound amines and aldehyde. Along with these, a number of major features related to the structure characteristics of glutaraldehyde were observed. These peculiar bands comprise the typical stretching bands of 2875 $cm^{-1}$ (H-C=O) and the much stronger alkyl bending and stretching vibrations at 1446 $cm^{-1}$ and 2960 $cm^{-1}$ (Figure 3b; Supporting Information, Figure S5e).[16c] On the other hand, XPS experiments further revealed the emergence of the new C 1s peak with the binding energy of 285.3 eV, which should be attributed to the alkyl carbon atoms from the glutaraldehyde unit (Supporting Information, Figure S3f). Collectively, both FTIR and XPS results consistently demonstrate the unambiguous immobilization of glutaraldehyde, thus providing additional aldehyde group available for the following protein incorporation through the same condensation as demonstrated above. Finally, by carefully applying this procedure to the nanogaps, we were able to integrate individual H1N1 antibodies into electrical circuits. The AFM image shown in Figure 3d (inset) confirms the presence of a single attached H1N1 antibody (ca. 20 nm in size), which is distinguishable when attached to a circa 30 nm-diameter SiNW.

Remarkably, by using the fresh antibody-decorated SiNW transistors in combination with microfluidics (Figure 4a), we realized rapid, direct, reversible electrical detection of H1N1 virus with high selectivity and single-molecule sensitivity. To decrease the measurement noises, we used a lock-in amplifier that was operated with a modulation frequency of 79 Hz. Signal amplification was achieved by attaching charged H1N1 HA antigens through the microfluidic system on the surface of the anchored H1N1 antibody and then electrostatically gating the underlying SiNW transistor. Attaching/deattaching antigen with antibody creates reversible changes in the electrostatic potential that dynamically modulate the electron fluxes through the conductive channel. The device was firstly stabilized by flowing deionized water (DI water, 18.2 MΩ m) at a flow rate of 0.2 mL $min^{-1}$ for about 200 s. Then, we sequentially delivered the analyte buffer solutions with different concentrations (7.8 pg $mL^{-1}$, 78 pg $mL^{-1}$, and 780 pg $mL^{-1}$), which were made by adding different amounts of H1N1 HA antigens to the constant PBS buffer solution, to the detection system. This injection resulted in a sudden increase in conductance (Figure 4b, black). These changes in conductance originate from two aspects: stochastic antibody/antigen interaction and nonspecific ion absorption, rather than either Schottky barrier modification (as discussed previously) or nonspecific antigen absorption (as demonstrated below). Interestingly, we found that further delivery of DI water could rinse both antigens and ions from the microchannel, thus causing the complete recovery of the original conductance of the devices. Therefore, it is not surprising that repeating the same above-used operations leads to the good reversibility of biosensing in our system (Figure 4b; Supporting Information, Figure S6a,b). Considering the fact that addition of antigen (stored in the PBS buffer solution) may change ion concentrations in the resulted buffer solution, which could influence the device conductance, we carried out control experiments by using the buffer solutions obtained by correspondingly adding the same

  

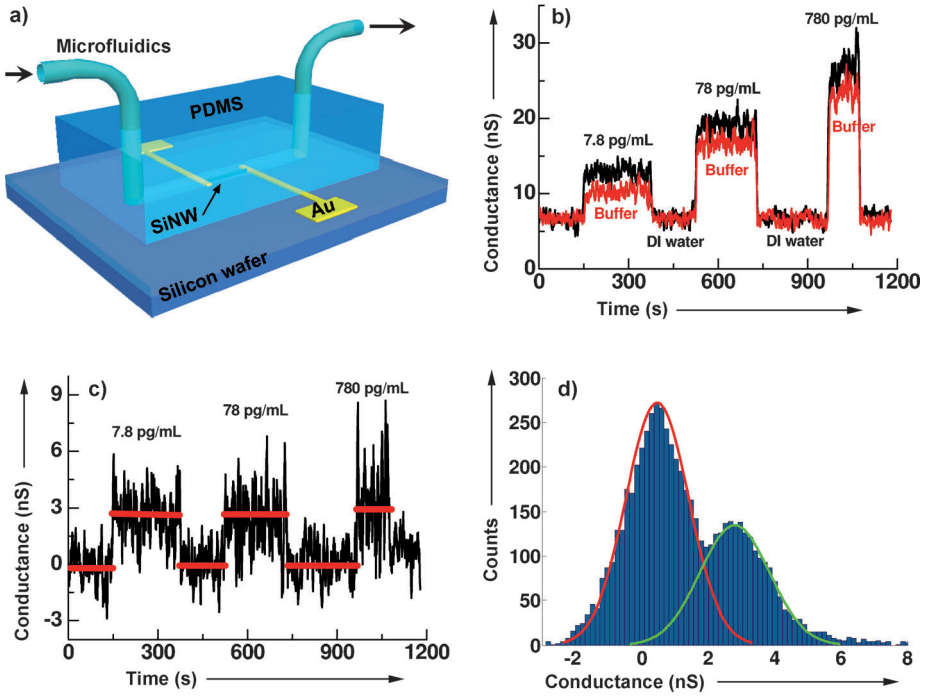


***Figure 4.*** a) Representation of the experimental setup with a microfluidic system. b) Conductance versus time plots for an antibody-decorated single-molecule device upon alternate additions of the solutions with different antigen concentrations (from 7.8 pg mL$^{-1}$ to 78 pg mL$^{-1}$ and 780 pg mL$^{-1}$, black) and the corresponding buffer solutions (red). $V_d = 50$ mV and $V_g = 0$ mV. c,d) Net changes in conductance after removing the influence of the buffer solutions and corresponding conductance-based histograms. The two levels are fit to Gaussian distributions (red line: deionized water; green line: antigen).

amounts of the solution used for storing antigens but without antigen under the same conditions (Figure 4b, red). To simplify further analysis and extract the net influence from antibody/antigen interactions, we removed the changes in conductance resulting from nonspecific ion absorption. As shown in Figure 4c and d, large-amplitude two-level fluctuations with a conductance difference of about 3 nS were observed. The most important thing we found is that at very low antigen concentrations, reversible electrical measurements on the same device did show essentially equivalent conductance changes, thus demonstrating no concentration dependence. This fact proves that these devices can monitor protein–protein interactions at the single-event level,[4a,d,e,13] which distinguishes this method as a unique platform from previous reports where nanotubes and nanowires were used to detect bulky proteins with concentration dependence.[11b,22] In comparison with the detection sensitivity from previous reports, such as ELISA sandwich arrays (ca. 3 pg mL$^{-1}$),[23] SPR (10–100 pg mL$^{-1}$),[24] nanowires arrays (ca. 0.9 pg mL$^{-1}$),[11b] and microcantilevers (ca. 0.2 ng mL$^{-1}$),[25] this method reaches the ultimate goal of real single-molecule sensitivity. To rule out potential artifacts from nonspecific absorption of antigens on the surface of SiNWs, we performed control experiments by using SiNWs without antibody decoration. We did not observe any net conductance at different antigen concentrations (Supporting Information, Figure S6a). To prove the selectivity, we replaced H1N1 HA antigen by 8 iso PGF 2a antigen, another similar protein which does not selectively interact with H1N1 antibody under the same conditions. None of the working devices showed obvious conductance changes upon treatments of 8 iso PGF 2a antigen with different concentrations in comparison with that of pure buffer treatment (Supporting Information, Figure S6b).

In conclusion, we have detailed a reliable method where assembly chemistry is interfaced with micro/nanofabrication techniques for developing SiNW-based single-molecule electrical biosensors. By taking advantage of the nature of the 1D core–shell structure of SiNWs, we lithographically created functional nanogaps for programmed point decoration and subsequent biocompatible assembly. Because these electrical biosensors have only one or at most two available spaces for protein accommodation, in combination with microfluidics, we achieved real-time, label-free, reversible electrical detection of protein-protein interactions with high selectivity, which reaches real single-molecule sensitivity. In comparison with more conventional optical techniques, this nanocircuit-based architecture is complementary but obviously with the advantages, such as no bleaching problem and no fluorescent labeling. These advantages clearly offer a platform for exploring dynamics of stochastic processes in biological systems and gaining information from genomics to proteomics to improve accurate molecular and even point-of-care clinical diagnosis. Furthermore, the proven reliability and ability to integrate these hybrid devices into current complementary metal oxide semiconductor (CMOS) technologies have the potential to make low-cost, portable detection arrays as a significant step towards practical electrical biosensors.

Received: October 30, 2013
Revised: January 18, 2014
Published online: March 25, 2014

**Keywords:** biosensors · H1N1 antibody · point decoration · silicon nanowires · single-molecule studies

[1] a) F. Patolsky, G. F. Zheng, C. M. Lieber, *Nat. Protoc.* **2006**, *1*, 1711–1724; b) S. Liu, Q. Shen, Y. Cao, L. Gan, Z. X. Wang, M. L. Steigerwald, X. F. Guo, *Coord. Chem. Rev.* **2010**, *254*, 1101–1116; c) B. L. Allen, P. D. Kichambare, A. Star, *Adv. Mater.* **2007**, *19*, 1439–1451; d) G. Gruner, *Anal. Bioanal. Chem.* **2006**, *384*, 322–335; e) K. I. Chen, B. R. Li, Y. T. Chen, *Nano Today* **2011**, *6*, 131–154; f) Y. X. Huang, P. Chen, *Adv. Mater.*

  

**2010**, *22*, 2818 – 2823; g) S. Liu, X. F. Guo, *NPG Asia Mater.* **2012**, *4*, e23.

[2] a) W. Yang, K. R. Ratinac, S. P. Ringer, P. Thordarson, J. J. Gooding, F. Braet, *Angew. Chem.* **2010**, *122*, 2160 – 2185; *Angew. Chem. Int. Ed.* **2010**, *49*, 2114 – 2138; b) S. Howorka, Z. Siwy, *Chem. Soc. Rev.* **2009**, *38*, 2360 – 2384; c) X. F. Guo, *Adv. Mater.* **2013**, *25*, 3397 – 3408; d) C. C. Jia, X. F. Guo, *Chem. Soc. Rev.* **2013**, *42*, 5642 – 5660.

[3] a) N. L. Rosi, C. A. Mirkin, *Chem. Rev.* **2005**, *105*, 1547 – 1562; b) J. W. Liu, Z. H. Cao, Y. Lu, *Chem. Rev.* **2009**, *109*, 1948 – 1998.

[4] a) X. F. Guo, J. P. Small, J. E. Klare, Y. L. Wang, M. S. Purewal, I. W. Tam, B. H. Hong, R. Caldwell, L. M. Huang, S. O'Brien, J. M. Yan, R. Breslow, S. J. Wind, J. Hone, P. Kim, C. Nuckolls, *Science* **2006**, *311*, 356 – 359; b) X. F. Guo, A. Whalley, J. E. Klare, L. M. Huang, S. O'Brien, M. Steigerwald, C. Nuckolls, *Nano Lett.* **2007**, *7*, 1119 – 1122; c) X. F. Guo, A. A. Gorodetsky, J. Hone, J. K. Barton, C. Nuckolls, *Nat. Nanotechnol.* **2008**, *3*, 163 – 167; d) S. Liu, G. H. Clever, Y. Takezawa, M. Kaneko, K. Tanaka, X. F. Guo, M. Shionoya, *Angew. Chem.* **2011**, *123*, 9048 – 9052; *Angew. Chem. Int. Ed.* **2011**, *50*, 8886 – 8890; e) S. Liu, X. Y. Zhang, W. X. Luo, Z. X. Wang, X. F. Guo, M. L. Steigerwald, X. H. Fang, *Angew. Chem.* **2011**, *123*, 2544 – 2550; *Angew. Chem. Int. Ed.* **2011**, *50*, 2496 – 2502; f) H. F. Wang, N. B. Muren, D. Ordinario, A. A. Gorodetsky, J. K. Barton, C. Nuckolls, *Chem. Sci.* **2012**, *3*, 62 – 65; g) S. Roy, H. Vedala, A. D. Roy, D. H. Kim, M. Doud, K. Mathee, H. K. Shin, N. Shimamoto, V. Prasad, W. B. Choi, *Nano Lett.* **2008**, *8*, 26 – 30.

[5] a) F. Patolsky, G. F. Zheng, O. Hayden, M. Lakadamyali, X. W. Zhuang, C. M. Lieber, *Proc. Natl. Acad. Sci. USA* **2004**, *101*, 14017 – 14022; b) B. Z. Tian, T. Cohen-Karni, Q. Qing, X. J. Duan, P. Xie, C. M. Lieber, *Science* **2010**, *329*, 830 – 834; c) E. Stern, J. F. Klemic, D. A. Routenberg, P. N. Wyrembak, D. B. Turner-Evans, A. D. Hamilton, D. A. LaVan, T. M. Fahmy, M. A. Reed, *Nature* **2007**, *445*, 519 – 522.

[6] a) Y. K. Choi, I. S. Moody, P. C. Sims, S. R. Hunt, B. L. Corso, I. Perez, G. A. Weiss, P. G. Collins, *Science* **2012**, *335*, 319 – 324; b) Y. Choi, T. J. Olsen, P. C. Sims, I. S. Moody, B. L. Corso, M. N. Dang, G. A. Weiss, P. G. Collins, *Nano Lett.* **2013**, *13*, 625 – 631; c) P. C. Sims, I. S. Moody, Y. Choi, C. J. Dong, M. Iftikhar, B. L. Corso, Q. T. Gul, P. G. Collins, G. A. Weiss, *J. Am. Chem. Soc.* **2013**, *135*, 7861 – 7868; d) S. Sorgenfrei, C. Y. Chiu, R. L. Gonzalez, Y. J. Yu, P. Kim, C. Nuckolls, K. L. Shepard, *Nat. Nanotechnol.* **2011**, *6*, 126 – 131; e) S. Sorgenfrei, C. Y. Chiu, M. Johnston, C. Nuckolls, K. L. Shepard, *Nano Lett.* **2011**, *11*, 3739 – 3743.

[7] a) H. Bayley, P. S. Cremer, *Nature* **2001**, *413*, 226 – 230; b) L. Soleymani, Z. C. Fang, E. H. Sargent, S. O. Kelley, *Nat. Nanotechnol.* **2009**, *4*, 844 – 848.

[8] a) H. T. Liu, J. He, J. Y. Tang, H. Liu, P. Pang, D. Cao, P. Krstic, S. Joseph, S. Lindsay, C. Nuckolls, *Science* **2010**, *327*, 64 – 67; b) X. C. Qin, Q. Z. Yuan, Y. P. Zhao, S. B. Xie, Z. F. Liu, *Nano Lett.* **2011**, *11*, 2173 – 2177.

[9] a) J. D. Wang, Z. X. Wang, Q. C. Li, L. Gan, X. J. Xu, L. D. Li, X. F. Guo, *Angew. Chem.* **2013**, *125*, 3453 – 3457; *Angew. Chem. Int. Ed.* **2013**, *52*, 3369 – 3373; b) Y. Cui, Z. H. Zhong, D. L. Wang, W. U. Wang, C. M. Lieber, *Nano Lett.* **2003**, *3*, 149 – 152; c) Y. Cui, L. J. Lauhon, M. S. Gudiksen, J. F. Wang, C. M. Lieber, *Appl. Phys. Lett.* **2001**, *78*, 2214 – 2216.

[10] a) Y. Cui, Q. Q. Wei, H. K. Park, C. M. Lieber, *Science* **2001**, *293*, 1289 – 1292; b) F. X. Shen, J. D. Wang, Z. Q. Xu, Y. Wu, Q. Chen, X. G. Li, X. Jie, L. D. Li, M. S. Yao, X. F. Guo, T. Zhu, *Nano Lett.* **2012**, *12*, 3722 – 3730; c) F. X. Shen, M. M. Tan, Z. X. Wang, M. S. Yao, Z. Q. Xu, Y. Wu, J. D. Wang, X. F. Guo, T. Zhu, *Environ. Sci. Technol.* **2011**, *45*, 7473 – 7480.

[11] a) E. Stern, A. Vacic, N. K. Rajan, J. M. Criscione, J. Park, B. R. Ilic, D. J. Mooney, M. A. Reed, T. M. Fahmy, *Nat. Nanotechnol.* **2010**, *5*, 138 – 142; b) G. F. Zheng, F. Patolsky, Y. Cui, W. U. Wang, C. M. Lieber, *Nat. Biotechnol.* **2005**, *23*, 1294 – 1301.

[12] a) G. F. Zheng, W. Lu, S. Jin, C. M. Lieber, *Adv. Mater.* **2004**, *16*, 1890 – 1893; b) B. Z. Tian, X. L. Zheng, T. J. Kempa, Y. Fang, N. F. Yu, G. H. Yu, J. L. Huang, C. M. Lieber, *Nature* **2007**, *449*, 885 – 888.

[13] a) Y. Cao, S. H. Dong, S. Liu, Z. F. Liu, X. F. Guo, *Angew. Chem.* **2013**, *125*, 3998 – 4002; *Angew. Chem. Int. Ed.* **2013**, *52*, 3906 – 3910; b) C. C. Jia, J. D. Wang, C. J. Yao, Y. Cao, Y. W. Zhong, Z. R. Liu, Z. F. Liu, X. F. Guo, *Angew. Chem.* **2013**, *125*, 8828 – 8832; *Angew. Chem. Int. Ed.* **2013**, *52*, 8666 – 8670; c) Y. Cao, S. H. Dong, S. Liu, L. He, L. Gan, X. M. Yu, M. L. Steigerwald, X. S. Wu, Z. F. Liu, X. F. Guo, *Angew. Chem. Int. Ed.* **2012**, *51*, 12228 – 12232.

[14] A. Witvrouw, B. Du Bois, P. De Moor, A. Verbist, C. Van Hoof, H. Bender, K. Baert in *Micromachining and Microfabrication Process Technology Vi*, *Vol. 4174* (Eds.: J. M. Karam, J. Yasaitis), Spie-Int. Soc Optical Engineering, Bellingham, **2000**, pp. 130 – 141.

[15] A. San Paulo, R. Garcia, *Biophys. J.* **2000**, *78*, 1599 – 1605.

[16] a) Q. Y. Sun, L. de Smet, B. van Lagen, M. Giesbers, P. C. Thune, J. van Engelenburg, F. A. de Wolf, H. Zuilhof, E. J. R. Sudholter, *J. Am. Chem. Soc.* **2005**, *127*, 2514 – 2523; b) B. J. Eves, Q. Y. Sun, G. P. Lopinski, H. Zuilhof, *J. Am. Chem. Soc.* **2004**, *126*, 14318 – 14319; c) Y. Li, S. Calder, O. Yaffe, D. Cahen, H. Haick, L. Kronik, H. Zuilhof, *Langmuir* **2012**, *28*, 9920 – 9929.

[17] Y. Ito, A. A. Virkar, S. Mannsfeld, J. H. Oh, M. Toney, J. Locklin, Z. N. Bao, *J. Am. Chem. Soc.* **2009**, *131*, 9396 – 9404.

[18] a) J. M. Buriak, M. J. Allen, *J. Am. Chem. Soc.* **1998**, *120*, 1339 – 1340; b) A. B. Sieval, A. L. Demirel, J. W. M. Nissink, M. R. Linford, J. H. van der Maas, W. H. de Jeu, H. Zuilhof, E. J. R. Sudholter, *Langmuir* **1998**, *14*, 1759 – 1768; c) M. R. Linford, P. Fenter, P. M. Eisenberger, C. E. D. Chidsey, *J. Am. Chem. Soc.* **1995**, *117*, 3145 – 3155.

[19] a) J. M. Buriak, M. P. Stewart, T. W. Geders, M. J. Allen, H. C. Choi, J. Smith, D. Raftery, L. T. Canham, *J. Am. Chem. Soc.* **1999**, *121*, 11491 – 11502; b) B. Paizs, B. J. Bythell, P. Maitre, *J. Am. Soc. Mass Spectrom.* **2012**, *23*, 664 – 675; c) A. Barth, *Prog. Biophys. Mol. Biol.* **2000**, *74*, 141 – 173.

[20] a) N. S. Bhairamadgi, S. Gangarapu, M. A. C. Campos, J. M. J. Paulusse, C. J. M. van Rijn, H. Zuilhof, *Langmuir* **2013**, *29*, 4535 – 4542; b) A. Khaliq, D. Pierucci, H. Tissot, J. J. Gallet, F. Bournel, F. Rochet, M. Silly, F. Sirotti, *J. Phys. Chem. C* **2012**, *116*, 12680 – 12686; c) X. Wallart, C. H. de Villeneuve, P. Allongue, *J. Am. Chem. Soc.* **2005**, *127*, 7871 – 7878.

[21] X. A. Zhao, C. W. Ong, Y. C. Tsang, Y. W. Wong, P. W. Chan, C. L. Choy, *Appl. Phys. Lett.* **1995**, *66*, 2652 – 2654.

[22] a) R. J. Chen, S. Bangsaruntip, K. A. Drouvalakis, N. W. S. Kam, M. Shim, Y. M. Li, W. Kim, P. J. Utz, H. J. Dai, *Proc. Natl. Acad. Sci. USA* **2003**, *100*, 4984 – 4989; b) K. Maehashi, T. Katsura, K. Kerman, Y. Takamura, K. Matsumoto, E. Tamiya, *Anal. Chem.* **2007**, *79*, 782 – 787; c) H. R. Byon, H. C. Choi, *J. Am. Chem. Soc.* **2006**, *128*, 2188 – 2189.

[23] A. M. Ward, J. W. F. Catto, F. C. Hamdy, *Ann. Clin. Biochem.* **2001**, *38*, 633 – 651.

[24] C. Campagnolo, K. J. Meyers, T. Ryan, R. C. Atkinson, Y. T. Chen, M. J. Scanlan, G. Ritter, L. J. Old, C. A. Batt, *J. Biochem. Biophys. Methods* **2004**, *61*, 283 – 298.

[25] G. H. Wu, R. H. Datar, K. M. Hansen, T. Thundat, R. J. Cote, A. Majumdar, *Nat. Biotechnol.* **2001**, *19*, 856 – 860.

  